Hindawi
Adsorption Science & Technology
Volume 2021, Article ID 6655227, 15 pages
https://doi.org/10.1155/2021/6655227

Research Article

Magnetite Functionalized *Nigella Sativa* Seeds for the Uptake of Chromium(VI) and Lead(II) Ions from Synthetic Wastewater

Patience Mapule Thabede, Ntaote David Shooto, Thokozani Xaba, and Eliazer Bobby Naidoo

Applied Chemistry and Nano-Science Laboratory, Department of Chemistry, Vaal University of Technology, P.O. Box X021, Vanderbijlpark 1900, South Africa

Correspondence should be addressed to Patience Mapule Thabede; mapulepseabelo@gmail.com

Received 25 July 2020; Accepted 14 December 2020; Published 12 January 2021

Academic Editor: Danina Krajišnik

The aim of the present study was to utilise pristine and magnetite-sucrose functionalized *Nigella Sativa* seeds as the adsorbents for the uptake of chromium(VI) and lead(II) ions from synthetic wastewater. Prestine *Nigella Sativa* seeds were labelled (PNS) and magnetite-sucrose functionalized *Nigella Sativa* seeds (FNS). The PNS and FNS composites were characterized by Fourier-transform infrared spectroscopy (FTIR) and X-ray powder diffraction (XRD). The FTIR analysis of both adsorbents revealed the presence of vibrations assigned to 1749 and 1739 cm^{-1} (-C=O) for ketonic group for both adsorbents. The amide (-NH) peak was observed at 1533 and 1527 cm^{-1} on FNS and PNS composites, respectively, whilst the carboxyl group (-COOH) were observed at 1408 cm^{-1} on both adsorbents. The XRD results of FNS and PNS composites showed a combination of spinel structure and y-Fe_2O_3 phase confirming the formation of iron oxide. The influence of operational conditions such as initial concentration, temperature, pH, and contact time was determined in batch adsorption system. The kinetic data of Cr(VI) and Pb(II) ions on both adsorbents was described by pseudo-first-order (PFO) model which suggested physisorption process. The sorption rate of Cr(VI) ions was quicker, it attained equilibrium in 20 min, and the rate of Pb(II) ions was slow in 90 min. Freundlich isotherm described the mechanism of Pb(II) ions adsorption on PNS and FNS composites. Langmuir best fitted the uptake of Cr(VI) ions on PNS and FNS. The results for both adsorbents showed that the removal uptake of Pb(II) ions increased when the initial concentration was increased; however, Cr(VI) uptake decreased when the initial concentration increased. The adsorption of Cr(VI) and Pb(II) ions on both adsorbents increased with temperature.

1. Introduction

Chromium compounds find their way into the natural water stream as a consequence of the industrialization and improper disposal of wastes which is usually from leather tanning, metal finishing, electroplating, and pigments industries [1]. Hexavalent chromium is one of the most contaminant that has attracted extensive attention among researchers due to its toxicity. Shupack [2] indicated that hexavalent chromium Cr(VI) species may occur in different ionic forms, namely chromate (CrO_4^{2-}), dichromate ($Cr_2O_7^{2-}$), or hydrogen chromate ($HCrO_4^-$) in aqueous solution; meanwhile, Cr(III) tends to form hydrated species such as hydrated trivalent chromium $[Cr(H_2O)_6]^{3+}$, chromium hydroxide complexes $[Cr(OH)(H_2O)_5]^{2+}$, or $Cr(OH)_2(H_2O)$. According to ([3] : 671), Cr(III) species are fairly less toxic as compared to Cr(VI) which is extremely toxic. The World Health Organisation (WHO) has restricted the limit of Cr(VI) to 0.05 mg/L in drinking water [4]. On the other hand, [5] : 1 reported that industries release effluent from batteries, automobile manufacturing units, and paint which contain lead Pb(II) ions. Pb(II) is one of the most toxic ions found in industrial wastewater [6]. The presence of lead Pb(II) ions in water is another major concerned because it affects human health, aquatic animals, peripheral nervous system, anaemia, loss of appetite, vomiting, severe abdominal

pain, and paralysis in the muscles [5, 6]. Pb(II) is a slow, malicious, but the most evil poison, where any path or level of contact can replace calcium on the bones and accrues in the skeletal system [7]. World Health Organization (WHO) assessment document indicated the safe level for lead ion concentration in blood to be 0.1 gm^{-3} [8].

Treatment of contaminated water using nanoparticles/-composites materials has been investigated by other researches, because magnetic composite adsorbents have become desirable materials for separating the loaded pollutant adsorbents from water post adsorption, and also, centrifugation and filtration can be time consuming and a costly process [9, 10]. Particles of hydroxides and iron oxides occurs in natural aquatic system and can adsorb anions and cations from aqueous system due to surface defects besides high magnetic character [11]. The following composites were used as adsorbents for removing different toxic ions in water. Some of the composites are catalytic oxidation and adsorption of Cr(III) on iron-manganese nodules under toxic conditions ; hematite iron oxide nanoparticles (α-Fe_2O_3), synthesis and modelling adsorption of malachite green ([12]); boron removal and reclamation by magnetic magnetite (Fe_3O_4) nanoparticle, an adsorption and isotopic separation study [13]; and scavenging of aqueous toxic organic and inorganic cations using novel facile magneto-carbon black-clay composite adsorbent [10].

However, there are few studies where composite material using *Nigella Sativa* seeds as adsorbents have been investigated. Some of these studies are *Nigella Sativa* plant-based nanocomposite-$MnFe_2O_4$/BC, an antibacterial material for water purification [14] with a maximum adsorption capacity of 10.07 mg/g for methylene blue. Nanohybrid composite Fe_2O_3-ZrO_2/BC for inhibiting the growth of bacteria and adsorptive removal of arsenic and dyes from water [15], the results showed that the removal of As(II) was 1.01 and 38.10 mg/g for methylene blue. *Nigella Sativa* seed-based nanohybrid composite-Fe_2O_3-SnO_2/BC is a novel material for enhanced adsorptive removal of methylene blue from water [16] with maximum adsorption capacity between 58.82 and 84.74 mg/g, and *Nigella Sativa* seed-based nanocomposite-MnO_2/BC is an antibacterial material for photocatalytic degradation and adsorptive removal of methylene blue from water which showed adsorption capacity of 185 mg/g [17].

Sucrose is a natural disaccharide which is formed from the combination of glucose and fructose [18]. Kuznetsov et al., [19] functionalized nanocarbons by a one-step process of fluorine substitution reaction with sucrose-derived lithium monosucrate. This was achieved by sonication in dimethylyformamide at room temperature. Their results showed that sucrose bonded on the surface of the fluorinated nanocarbons using covalent bonding. Functionalization of multiwalled carbon nanotubes (MWCNTs) with D-sucrose carbohydrate was done by [20] in water at room temperature. Their aim was to investigate the influence of sucrose on MWCNTs surface and morphology using polyamide-imide (PAI) nanocomposites. Obark and Obark, [21] investigated the capability of activated carbon for the removal of chromium(VI) ions by adding sucrose in the adsorption as an organic matter.

Technologies can be more effective if and when the adsorbent could be prepared easily, cost effectively, and effective for range of pollutants. They should also be effective for the removal of high and low level of pollutants [22]. Also, WHO (World Health Organization) emphasised on the investigation of medicinal plant species for human care system benefit [23]. Therefore, the present work was made to prepare a material, with low cost, which can remove chromium(VI) and lead(II) ions from aqueous solution. Plant materials are abundant and sustainable and may provide oxygenous groups which can interact with charged pollutants from water without harming water quality [24]. Black cumin seeds (BCS) (*Nigella Sativa*) are used as home medicine and have bitter taste and smell [25]. It is used primarily in confectionery and liquors as well for medicinal purposes. The efficiency of *Nigella Sativa* was investigated for adsorption by seeing the challenges continuing in toxic ions removal and the benefits offered by the biomasses [26]. These seeds are readily available and inexpensive and have a number of oxygenous groups (carboxyl and hydroxyl) at the surface, which make them advantageous for the adsorption technology [27]. Some studies available in the literature have shown that *Nigella Sativa* material has been used for the adsorption studies. However, there is a need for some type of modifications in order to get more important results for the removal of water contaminants [28]. Accommodation of nanoparticles onto adsorbent surface and large number of functional groups of the material can provide the large vacant sites to nanocomposite for charged pollutants [29]. Inorganic nanomaterials have shown unique and extraordinary properties for numerous applications including adsorption [30, 31]. The preparation of such material is eco-friendly, has low production cost, and is nontoxic; this can be a better solution for water treatment. In view of these facts, magnetite was incorporated into the *Nigella Sativa* powder for the formation of magnetite *Nigella Sativa* seeds then functionalized with sucrose for chromium(VI) and lead(II) ions adsorption from aqueous solution.

Sucrose is an inexpensive, commercially available, and easily renewable carbon source [32]. Used magnetic ceramsite coated by functionalized nanocarbon spheres. Their study shows that using ceramsite without functionalization had low porosity, insufficient active site, and low adsorption capacity for the removal of Cr(VI). To improve the adsorption capacity, ceramsite was functionalized with magnetic nanocarbon spheres using sucrose. Their study also showed that there was an increased removal of Cr(VI) with an increased concentration of sucrose. Synthesis of graphene sand composite was prepared with the use of a sucrose [33]. Their composite exhibited a maximum adsorption capacity of 106.2 mg/g for the removal of Cr(VI) at pH 1.5. Mesoporous carbon was obtained by [34] using a silica material as a template and sucrose as a carbon precursor for the adsorption of anionic azo dyes. The results showed that adsorption of dyes ranged from 128 to 172 mg/g. Bedin et al., [35] prepared activated carbon from sucrose for the adsorption of methylene blue dye. Their work showed that the use of

sucrose in conjunction with chemical activation (KOH) to synthesize activated carbon had a high adsorption capacity (704 mg/g) for methylene blue. Thus, the use of sucrose as one way of modifying the adsorbents may improve adsorption capacity for the removal of toxic ions and dyes.

Previous work on *Nigella Sativa* seeds showed that the material has good removal uptake towards pollutants in water. Therefore, it is fair to conduct further studies on the material. Hence, the purpose of the present study was to develop functionalized *Nigella Sativa* seeds with enhanced removal uptake towards Cr(VI) and Pb(II) ions. In this study, the seeds were incorporated with sucrose and iron oxide to produce a composite material. The magnetic-sucrose functionalized *Nigella Sativa* (FNS) composite was a one-step process done at room temperature. Incorporation of sucrose and iron oxide has proven to enhance the adsorption capacity of the other materials; however, no document was found that investigated this for *Nigella Sativa* seeds.

2. Reagents and Experimental

2.1. Reagents. Sucrose ($C_{12}H_{22}O_{11}$), Iron(II) chloride ($FeCl_2{\cdot}4H_2O$), Iron (III) chloride ($FeCl_3{\cdot}6H_2O$), sodium thiosulfate ($Na_2S_2O_3$), potassium dichromate $K_2Cr_2O_7$, and lead nitrate $Pb(NO_3)_2$ were purchased Sigma-Aldrich, Johannesburg, South Africa. Other chemicals like ammonium hydroxide (NH_4OH), sodium hydroxide (NaOH), and hydrochloric acid (HCl) were purchased at Associated Chemical Enterprises, Johannesburg, South Africa. Unprocessed *Nigella Sativa* seeds were procured from a health shop in Vanderbijlpark, South Africa.

2.2. Preparation of Pristine Nigella Sativa (PNS) Composite. 100 g of pristine *Nigella Sativa seeds* was weighed thereafter rinsed in distilled water several times to get rid of dust and dirt. The seeds were dried in an oven at 40°C for 24 hr. After drying, the seeds were ground with a mortar and piston. The ground seeds were sieved on 60/200 mesh in order to get particle sizes ranging from 0.8 to 1 mm. The sieved pristine *Nigella Sativa* seeds were labelled (PNS).

2.3. Preparation of the Sucrose Functionalized Nigella Sativa (FNS) Composite. Pristine *Nigella Sativa* (PNS) seeds (10 g) were poured in a beaker, and 0.5% sucrose solution (50 mL) was mixed with the seeds. The sucrose functionalized *Nigella Sativa* (FNS) was stirred for 2 hr. Thereafter, $FeCl_3$ (5 g) was added which was allowed to mix for 3 hr followed by 5 g of $FeCl_2$. A 10 mL of 25% NH_4OH solution was added. When the solution becomes homogenous, 5 g $Na_2S_2O_3$ was added into the mixture. The resultant black yellowish magnetic FNS composite was continuously stirred for 3 hr. The obtained product was rinsed with distilled water and dried for 24 hr at 40°C. The prepared composite is shown in Scheme 1.

2.4. Batch Adsorption Experiments. To better understand the adsorption behaviour of the adsorbents, a number of batch studies were conducted to investigate the effect of pH, initial concentration, contact time, and temperature. Lead nitrate and potassium dichromate were used to prepare the stock solutions of 100 mg/L. A 0.1 g of the adsorbent and 40 mL of the working standard solutions were transferred to 100 mL capped plastic tubes. The solutions were then placed on a shaker for 60 min. Thereafter, the composites were separated by centrifugation for 5 min at 5000 rpm. For all the parameters, the supernatant was used for the analysis. The effect of pH was studied at 1, 3, 5, 7, and 9 using a standard solution of 100 mg/L and stirred for 60 min. Other adsorption studies conducted were time effect at 1, 5, 10, 15, 20, 30, 60, 90, and 120 min (using the same standard solution concentration for all other parameters). The effect of temperature was conducted at 298, 303, 313, 333, and 353 K, whilst the concentration was studied at 20, 40 60, 80, and 100 mg/L. The solution pHs ranging from 1 to 9 were adjusted by adding 0.1 M NaOH for basic medium and 0.1 M HCl for acidic medium. Thereafter, the adjusted pH solutions were added to 0.1 g adsorbents and agitated at 200 rpm for 24 hr. The point of zero charge (pH_{pzc}) determination of FNS and PNS was conducted using 1 M $NaNO_3$.

2.5. Data Management. The percentage removal of Cr(VI) and Pb(II) ions from aqueous solution onto FNS and PNS composites surface was determined by using the following equations (1) and (2) [36]:

$$q_e = \frac{(C_o - C_e)\,V}{W}, \tag{1}$$

$$\%R = \frac{(C_o - C_e)}{C_o} \times 100, \tag{2}$$

where C_o and C_e (mg/L) are initial and equilibrium concentrations of Cr(VI) and Pb(II) ions and q_e adsorption capacity (mgg^{-1}) and $\%R$ (%) of FNS and PNS composites at equilibrium. The volume of the solution and the mass of the adsorbents are labelled (v) in L and (w) in g, respectively.

2.5.1. Adsorption Isotherm Models. In order to better understand the interaction between the Cr(VI) and Pb(II) ions and the adsorbent surface, concentration data were used in nonlinear isotherm models, namely Langmuir (3) [37] and Freundlich (4) isotherms [38].

$$q_e = \frac{Q_o b C_e}{1 + bC_e}, \tag{3}$$

$$q_e = k_f C_e^{1/n}, \tag{4}$$

where Q_o represent Langmuir maximum adsorption capacity (in mg/g), b is the interaction energy-related constant, C_e (mgL^{-1}), (k_f) is Freundlich capacity factor constant, and ($1/n$) represent isotherm linearity parameter constant.

2.5.2. Adsorption Kinetics. Various kinetic models, namely pseudo-first-order (PFO) and pseudo-second-order (PSO) rate models [39] and intraparticle diffusion (IPD) [40] nonlinear equations as shown in equations (5), (6), and (7),

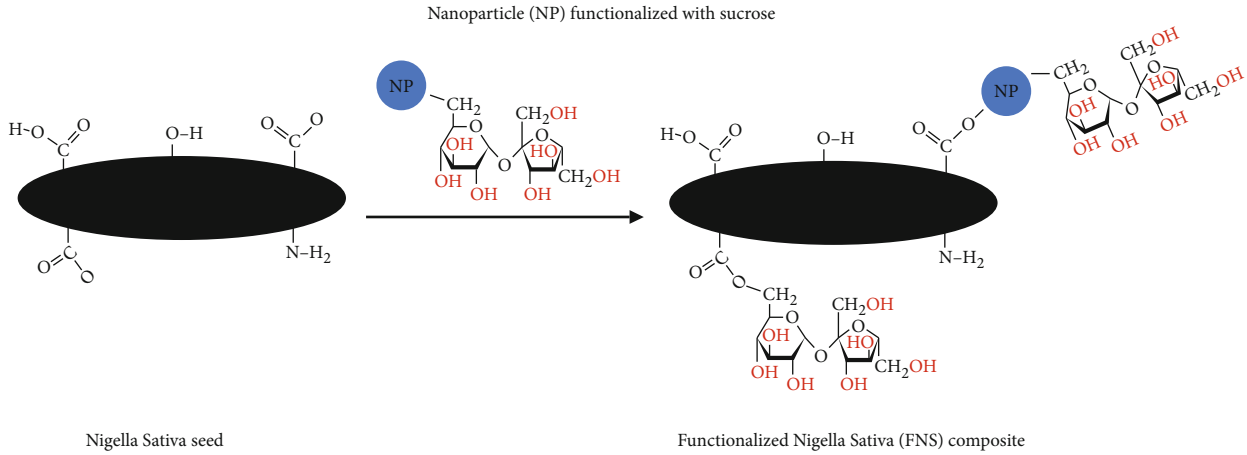

Scheme 1: Schematic of sucrose functionalized *Nigella Sativa* seeds (FNS) preparation.

respectively, were used on the obtained experimental data of Cr(VI) and Pb(II) ions at different time intervals.

$$q_e = q_t\left(1 - e^{-k_1 t}\right), \tag{5}$$

$$q_e = \frac{1 + k_2 q_e t}{k_2 q_e^2 t}, \tag{6}$$

$$q_t = k_i\left(t^{1/2}\right) + C, \tag{7}$$

where q_e and q_t represent the amounts removed (in mg/g) at time (t). (k_1), (k_2), and (k_i) are the rate constants of PFO (in min^{-1}), PSO (in g $\text{mg}^{-1}\,\text{min}^{-1}$), and IPD (in g $\text{g}^{-1}\,\text{min}^{1/2}$), respectively. C represents the concentration of Cr(VI) and Pb(II) ions at equilibrium.

2.5.3. Thermodynamic Functions. The investigation of the adsorption process was evaluated using thermodynamics calculation of enthalpy change (ΔH^o), entropy change (ΔS^o), Gibb's free energy change (ΔG^o), and the equilibrium constant (K_c) were determined at 298, 303, 313, 333, and 353 K by means of equations (8), (9), and (10) [41].

$$\text{In}\, K_c = -\frac{\Delta H^o}{RT} - \frac{\Delta S^o}{R}, \tag{8}$$

$$\Delta G^o = -RT\,\text{In}\, K_c, \tag{9}$$

$$K_c = \frac{q_e}{C_e}. \tag{10}$$

2.6. Instrumentation. The FNS and PNS composites were analysed for phase composition through the X-ray diffraction (XRD) with anode of Cu (Bruker, $\lambda = 1.5406$ Å) Shimadzu XRD 7000. The samples were scanned at $2\theta = 10 - 70^\circ$ with a scan rate of 10°/min. Thermo Fischer Scientific Fourier transform infrared (FTIR) spectroscopy was used to determine the spectra sorption materials from 4000 to 400 cm^{-1}. Atomic absorption spectroscopy (AAS) Shimadzu ASC 7000 with air-acetylene flame and autosampler was used to determine the remaining Cr(VI) and Pb(II) ions in aqueous solutions.

3. Results and Discussion

3.1. Characterization of the Adsorbents

3.1.1. FTIR Results. The FTIR spectra of prepared FNS and PNS composites characteristics absorption peaks at various wavenumbers ranging from 3238 to 812 cm^{-1} are shown in Figure 1. The broad peaks around 3228 and 1625 cm^{-1} were attributed to hydroxyl (-OH) groups [9] on FNS composite. These groups shifted to higher frequency of 3238 and 1631 cm^{-1} on PNS composite. The two sharp peaks at 2918 and 2849 cm^{-1} were attributed to C-H stretching vibrations of $-CH_3$ and $-CH_2$ groups, respectively, [42]. The bands at 1749 and 1739 cm^{-1} (-C=O) for ketonic group were observed for both FNS and PNS composites, respectively, [43]. The shift of the C=O stretch showed that there is effective interaction between sucrose adsorbents and the functional groups on the surface [20]. The (-NH) peak due to the amide was observed at 1533 and 1527 cm^{-1} on FNS and PNS composites, respectively, which were close to the previously reported by [43]. The carboxyl group (-COOH) on both adsorbents were observed at 1408 cm^{-1}. Other bands at 1243, 1157, and 1000 cm^{-1} of PNS and 1247, 1152, and 1001 cm^{-1} of FNS were attributed to structures of hemicellulose, cellulose, and lignin [44–46]. Therefore, the changes obtained from the FTIR spectrum of the functionalization black cumin seeds have indicated a number of functional groups on the surface of FNS and PNS composites which may propose that these functional groups were responsible for the Cr(VI) and Pb(II) ions adsorption from aqueous solutions.

The FT-IR spectra of PNS and FNS composites loaded with Pb(II) and Cr(VI) ions are compared with composites before adsorption as shown in Figures 1(b) and 1(c), respectively. The FT-IR spectrum of PNS (Figure 1(b)) after the adsorption of Pb(II) showed various functional groups at different frequencies. The peaks at 3238, 2918, and 2849 cm^{-1} shifted towards the 3273, 2921, and 2851 cm^{-1} after adsorption, whilst (-C=O) for ketonic group above 1700 cm^{-1}

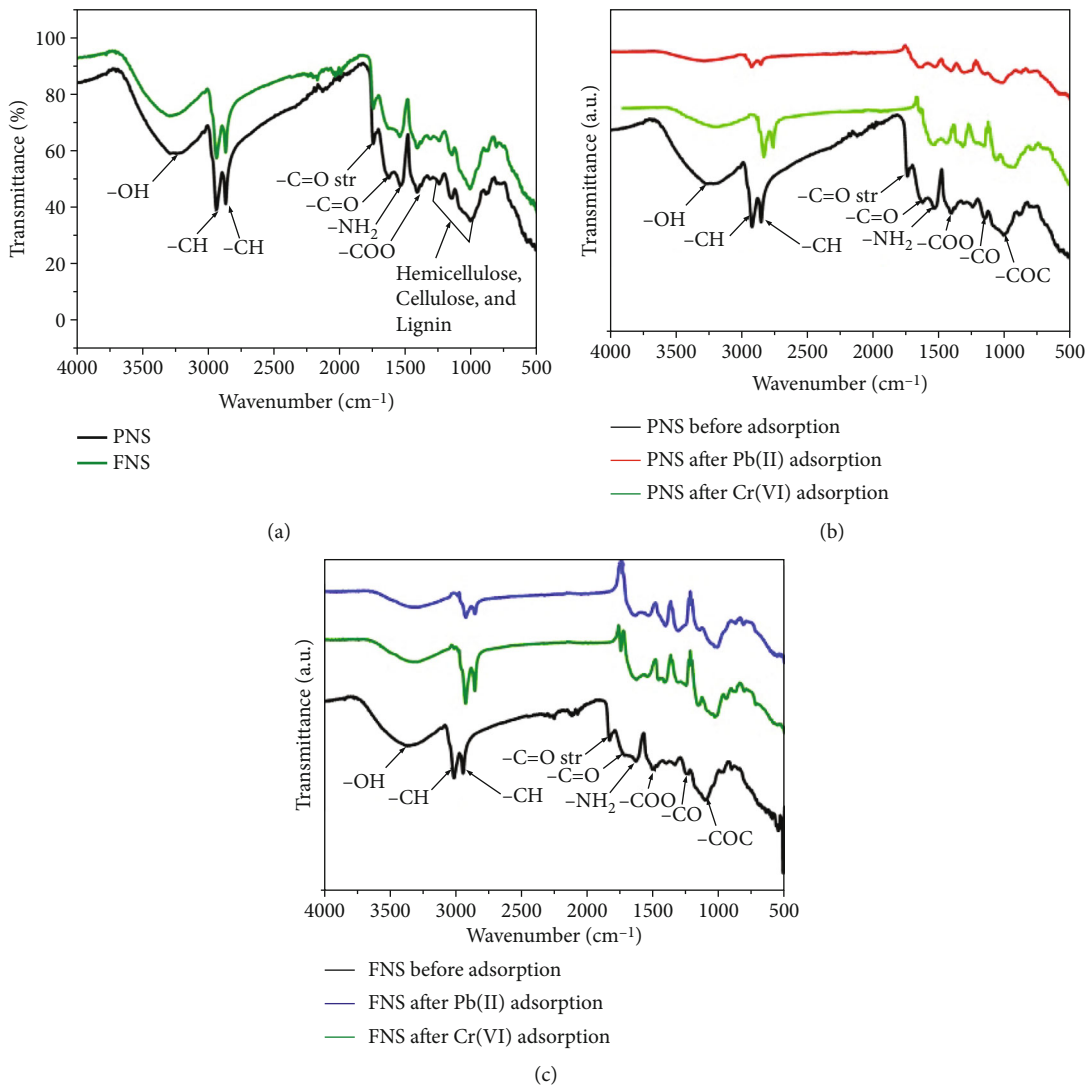

Figure 1: IR spectra of (a) PNS and FNS composites before adsorption, (b) PNS composite before and after adsorption, and (c) FNS composite before and after adsorption of Pb(II) ions and Cr(VI).

disappeared and the hydroxyl group at 1625 cm^{-1} shifted to 1627 cm^{-1}. The amide (-NH) peak observed at 1527 cm^{-1} shifted to 1528 cm^{-1}, whilst the (-COO) group shifted to 1405 cm^{-1} after the adsorption of Pb(II). The peaks associated with hemicellulose, cellulose, and lignin shifted to 1234, 1148, and 1011 cm^{-1}. The peaks obtained from the FT-IR adsorption spectrum of PNS loaded Cr(VI) are shown in Figure 1(b). The adsorption of Cr(VI) (Figure 1(b)) on the adsorbent showed that the functional groups had shifted to 3205, 2827, and 2757 cm^{-1}. However, the peak at 1739 cm^{-1} attributed to (-C=O) ketonic group and the peak due to hydroxyl group at 1631 cm^{-1} dropped off. On the other hand, the amide (-NH) at 1527 cm^{-1} shifted to 1535 cm^{-1}, whilst carboxyl group (-COOH) shifted from 1408 to 1436 cm^{-1}. There is a new peak at 1315 cm^{-1}, and the cellulosic framework shifted to 1153, 1061, and 930 cm^{-1} [9].

The FT-IR absorption spectra of FNS composites after adsorption of Pb(II) and Cr(VI) are shown in Figure 1(c). The peaks on FNS for Pb(II) at 3228 and 1625 cm^{-1} were assigned to hydroxyl (-OH) groups before adsorption, and the two sharp peaks at 2918 and 2849 cm^{-1} (-CH_3 and -CH_2) shifted to 3287, 1626, 2921, and 2852 cm^{-1} after adsorption, respectively. The (-C=O) band at 1749 cm^{-1} disappeared. The amide group observed at 1533 cm^{-1} shifted to 1532 cm^{-1}. The carboxyl group (-COOH) observed at 1408 cm^{-1} shifted to 1405 cm^{-1}, and the peak at 1247 disappeared. There was a new peak formed at 1308 cm^{-1}. The hemicellulose and cellulose peaks shifted to 1148 and 1009 cm^{-1}. The FNS spectrum loaded with Cr(VI) in Figure 1(c) showed that the hydroxyl groups and (-CH_3 and -CH_2) shifted to 3298, 1620, 2920, and 2852 cm^{-1}, respectively. The (-C=O) peak shifted to 1744 cm^{-1} with reduced intensity. The (-NH) peak at 1533 cm^{-1} shifted to 1535 cm^{-1}, whilst the (-COOH) peak shifted to 1455 cm^{-1} after adsorption. The hemicellulose and cellulose peaks shifted to 1245, 1150, and 1029 cm^{-1}. The intensity of peaks on PNS and FNS after the adsorption reduced significantly which may

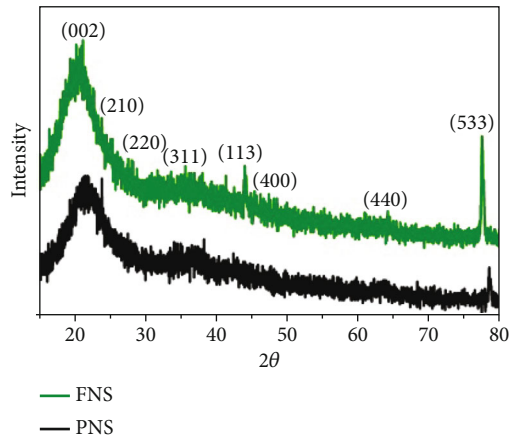

Figure 2: XRD spectra of FNS and PNS composites.

imply that there was interaction of oxygenous composites through electrostatic and hydrogen bonding [15].

3.1.2. XRD Results. The X-ray diffraction pattern of FNS and PNS composites is illustrated in Figure 2. The broad peak at (2θ) value between 15 and 25° indicated the cellulosic structure of the black cumin seed material [14]. The XRD spectra of FNS and PNS composites show peaks around 23.73°, 30.84°, 35.27°, 41.24°, 43.41°, 62.43°, and 77.48° corresponding to (210), (220), (311), (113), (400), (440), and (533) planes with combination of spinel structure and y-Fe_2O_3 phase confirming the formation of iron oxide [9, 47]. The FNS composite adsorbent showed that it had higher intensity peaks as compared to PNS composites.

3.2. Adsorption Studies

3.2.1. Effect of pH Solution. The adsorption of Cr(VI) and Pb(II) ions by FNS and PNS composites was evaluated at pH ranging from 1 to 9 as shown in Figures 3(a) and 3(b). The experimental data showed that the adsorption of Cr(VI) and Pb(II) ions was pH dependant. The sorption of Cr(VI) ions by PNS and FNS composites showed a decrease in capacity as the pH increased. A similar observation was recorded in the literature by [48] using macadamia nutshells. Lesaoana et al., [49]; He et al., [50] explained this trend by stating that at low pH (1-3), the hydrolysis reaction of dichromate ion ($Cr_2O_7^{2-}$) yields $HCrO_4^-$ which alternately becomes the main Cr(VI) species in acidic medium. However, at elevated pH, $HCrO_4^-$ causes the equilibrium to shift towards creating CrO_4^{2-} and $Cr_2O_7^{2-}$ species. It is further mentioned that at lower pH, the negatively charged dichromate or chromate binds electrostatically to the positively charged groups on the surface of the adsorbents because at low pH the surface of the adsorbents are positively charged due to protonation. Additionally, ([50] : 5) mentioned that this phenomenon was about the surface charge of the adsorbent and that the obtained modified adsorbent pHpzc ranged from 2 to 4 which was also observed in this study (Table 1). It is said that when the adsorbent is positively charged, it will adsorb anions containing Cr(VI), such as $HCrO^{4-}$ and $Cr_2O_7^{2-}$. Otherwise, when the adsorbent is negatively charged, it reduces the electrostatic interaction between the adsorbent and anionic Cr(VI). This means that pH is very important for the removal of Cr(VI) ions owing to its effects on the electrostatic interaction. A different trend was observed in the adsorption of Pb(II) ions whereby adsorption capacities of FNS and PNS composites increased as pH of the solution increased from pH 1 to pH 5; then, beyond pH 5, the adsorbed amount remained the same with a slight decrease. This is due to the fact that, as the pH increases, the H^+ ion in the solution decreases, therefore, the greater the number of negatively charged ions which makes the binding sites available for the metal adsorption to take place. The adsorption of Cr(VI) ions on both adsorbents was lower compared to Pb(II) ions due to electrostatic repulsion of hydroxyl ions which are negatively charged [48].

3.2.2. Speciation Diagrams of Cr(VI) and Pb(II) Ions. At different pH values, chromium exists in aqueous solution in different anionic forms, namely hydrogen chromate ($HCrO_4^-$), chromate (CrO_4^{2-}), chromic acid (H_2CrO_4), and dichromate ($Cr_2O_7^{2-}$) [51–53]. The speciation of these Cr(VI) anions depends on the concentration and pH of the solution [54, 55]. Figure 4(a) shows the speciation of Cr(VI) as a function of pH at a concentration of 100 mg/L. H_2CrO_4 belongs to the strong acids and is only observed below pH 1. However, at pH >1, deprotonated form of Cr(VI) was observed; hence, product $HCrO_4^-$ was formed at a pH from 1 to 6.5. The diagram shows that $HCrO_4^-$ was the major species at the experimental concentration, and this was dominant between pH 1 and 6.5. According to [56, 57], $HCrO_4^-$ is usually the most predominant Cr(VI) species at acidic conditions. A similar observation was reported by [58, 59] stating that $HCrO_4^-$ species usually formed around pH below 6.8. In our study, $HCrO_4^-$ form was obtained at pH 1; thereafter, the capacity started decreasing. This indicated that $HCrO_4^-$ prevails in acidic medium. The decrease in sorption capacity could be due to the depletion of protons subsequently less protonated sites and more hydroxide groups that may result in competition with CrO_4^{2-} ions for adsorption [57]. As the pH increased towards basic medium, only CrO_4^{2-} ions were in the solution throughout the concentration range ([60]; Markiewicz et al., 2014). On the other hand, $Cr_2O_7^{2-}$ is stable at weakly acidic and low oxidizing environments [57]. In our study, the metal ion concentration was ranging between 20 and 100 mg/L; hence, $Cr_2O_7^{2-}$ was not included in the diagram. Therefore, this may suggest that Cr(VI) existed mainly as $HCrO_4^-$ anion. Bhowal and Datta, [61]; Markiewicz et al., (2014); Zhang et al., [53] indicated that $Cr_2O_7^{2-}$ is dominant in more concentrated solution above 100 mg/L. Pakade et al. [48] have shown that at low pH of 2, there is a possibility of Cr(III) forming when using macadamia nutshell. However, as the pH increased from 3 to 9, Cr(III) and Cr(VI) also decreased. Yang and Chen, [62] also mentioned that at strongly acidic conditions Cr(VI) can be reduced to Cr(III). Therefore, it can be concluded that in this study only Cr(VI) was formed.

The pH of the solution is considered as the major parameter controlling metal speciation [63]. Figure 4(b) shows the

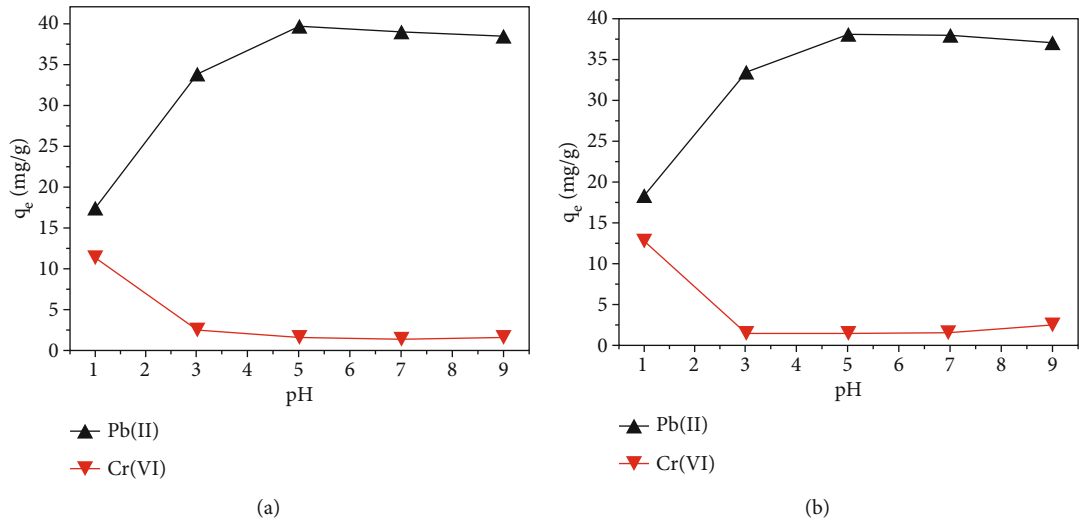

Figure 3: pH effect Onto (a) PNS and (b) FNS composites for Pb(II) ions and Cr(VI) sorption. Experimental conditions: volume of solution (40 mL), time (60 min), adsorbent dosage (0.1 g), temperature (298 K), agitation rate (200 rpm), and concentration (100 ppm).

Table 1: Maximum sorption capacities of previously reported various adsorbents for Pb(II) ions.

Adsorbent	Maximum capacity (mg/g)	Solution pH	Temperature (°C)	Reference
Magnetic coffee waste	41.2	6	25	Edathil et al., [83]
Magnetic cane biochar	40.6	5	20	Mohan et al., [84]
Fe_3O_4@SiO_2-IP polymer	32.6	4.8	25	Guo et al., [85]
Fe^{3+}/Fe^{2+} black cumin seeds	39.67	5	25	This study
Plums biochar	28.8	6	25	Pap et al., [86]
Dolomite	19.7	6	45	Irani et al., [87]
Apricot biochar	12.7	6	25	Pap et al., [86]
Wood biochar	7.9	5	25	Bardestani et al., [8]
Mushroom	3.9	6	25	Kariuki et al., [88]
Rice husk biochar	2.4	5	25	Liu and Zhang [41]

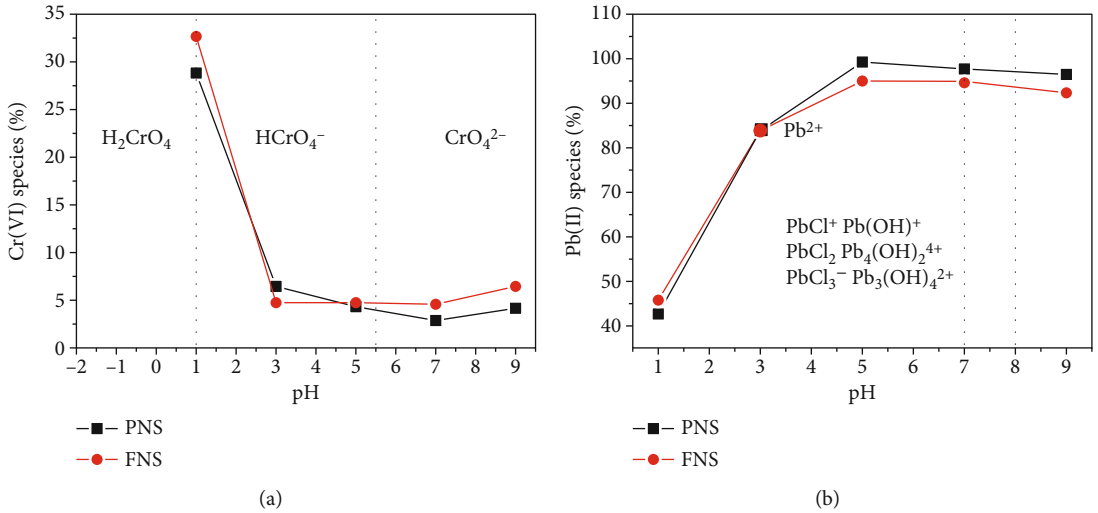

Figure 4: Speciation diagrams of (a) Cr(VI) and (b) Pb(II) ions onto PNS and FNS composites at a concentration of 100 mg/L at room temperature.

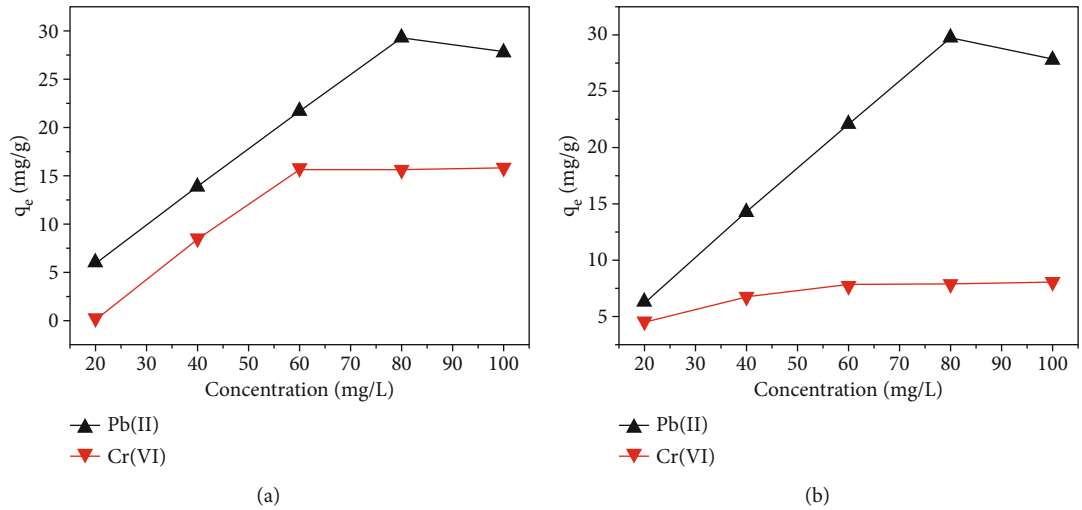

Figure 5: Concentration effect onto (a) PNS and (b) FNS composites for Pb(II) ions and Cr(VI) sorption. Experimental conditions: volume of solution (40 mL), time (60 min), adsorbent dosage (0.1 g), temperature of the system (298 K), agitation rate (200 rpm), and pH of solutions during Pb(II) ions and Cr(VI) sorption (5.0).

Table 2: Isotherms studies and their parameters.

Isotherms		FNS		PNS	
		Pb(II)	Cr(VI)	Pb(II)	Cr(VI)
Langmuir	Q_o (mgg^{-1})	19.99	10.21	12.06	15.11
	b (Lmg^{-1})	6.6301	0.0412	1.0751	0.0642
	r^2	0.9031	0.9973	0.9355	0.9952
Freundlich	$1/n$	22.783	48.654	19.791	4.425
	k_f ($mg^{(1-n)}\,L^n\,g^{-1}$)	0.730	6.589	0.684	1.322
	r^2	0.9961	0.893	0.9975	0.8869
Experimental (q_e) (mg/g)		29.80	7.80	29.47	15.74

species distribution diagram of Pb(II) in an aqueous solution against pH at a concentration of 100 mg/L. The results showed that higher sorption capacity was obtained between pH 2 and 5 where lead occurred only as Pb^{2+} species up to pH 6.0. This was also achieved in the research work done by [64]. Since HCl was used to adjust pH, it was suggested that there might be lead chloride complexes formation. From the diagram formation of lead chloride, complexes were obtained between pH 7.0 and 8.0. Lukanin et al., [65] showed that lead chloride species can be obtained around pH 7.3 and 8.3, whilst [66] data showed that lead chloride formed from pH 7.2 to 7.6. Above pH 7.5 to alkaline conditions, there was production of hydroxyl groups and consequently increased the amount of lead hydroxide solution [67, 68]. Silwamba et al., [69] have also showed that the addition of hydrochloric acid can form Pb^{2+} and lead chloride complexes such as $PbCl^+$, $PbCl_2$, and $PbCl_3^-$.

3.2.3. Concentration and Adsorption Isotherms. Figures 5(a) and 5(b) show the effect of initial concentrations on the adsorption of Cr(VI) and Pb(II) ions by PNS and FNS composites. The removal efficiency of both adsorbents was found to be dependent on the initial concentration of chromium. The adsorption of Pb(II) by PNS in Figure 4(a) increased with increasing concentration from 20 to 80 mg/L, whilst the adsorption of Cr(VI) increased from 20 to 60 mg/L. Thereafter, the removal efficacy slowly reached adsorption equilibrium, and there was no further increase in the adsorption of Cr(VI). A similar adsorption trend was observed for FNS in Figure 4(b) whereby Pb(II) ions adsorption increased with increasing initial concertation (20-80 mg/L). However, the adsorption of Cr(VI) ions stays almost constant as the initial concentration increases. The maximum adsorption capacities at initial concentration of 20 mg/L onto FNS in Figure 4(b) was 4.34 and 6.14 mg/g for Cr(VI) and Pb(II) ions, respectively, whereas on PNS, it was only 0.26 mg/g and 5.98 mg/g for Cr(VI) and Pb(II) ions, respectively. On the other hand, the maximum adsorption capacities at 100 mg/L onto PNS in Figure 4(a) for Pb(II) and Cr(VI) ions were 29.47 and 15.74 mg/g, respectively, then onto FNS in Figure 4(b) was observed at 29.80 and 7.80 mg/g for Pb(II) and Cr(VI), respectively. The results in both Figures 4(a) and 4(b) showed that both adsorbent capacities increased with increased initial concentration especially for Pb(II) ions. The reason why Pb(II) ions were adsorbed more than Cr(VI) ions on PNS and FNS composites might be due to negatively charged Cr(VI) ion electrostatically repelling the adsorbed ions resulting in a decrease of the adsorption capacity. Also, as seen in Figure 3, the maximum adsorption for Cr(VI) took place at pH 1. Thereafter, an increase in pH resulted to a decreased in adsorption due to $HCrO_4^-$, CrO_4^{2-}, and $Cr_2O_7^{2-}$ and decreased in surface protonation [70].

The interaction of Cr(VI) and Pb(II) ions with PNS and FNS composites surfaces adsorption mechanism and surface affinities towards Cr(VI) and Pb(II) ions is described with the help of nonlinear Langmuir and Freundlich isotherms. The adsorption isotherms and their parameters are shown in Table 2. The data showed that Pb(II) ions on PNS and FNS composites had (r^2) of 0.996 and 0.997 for Freundlich isotherms, whilst Langmuir isotherm showed r^2 of 0.903 and

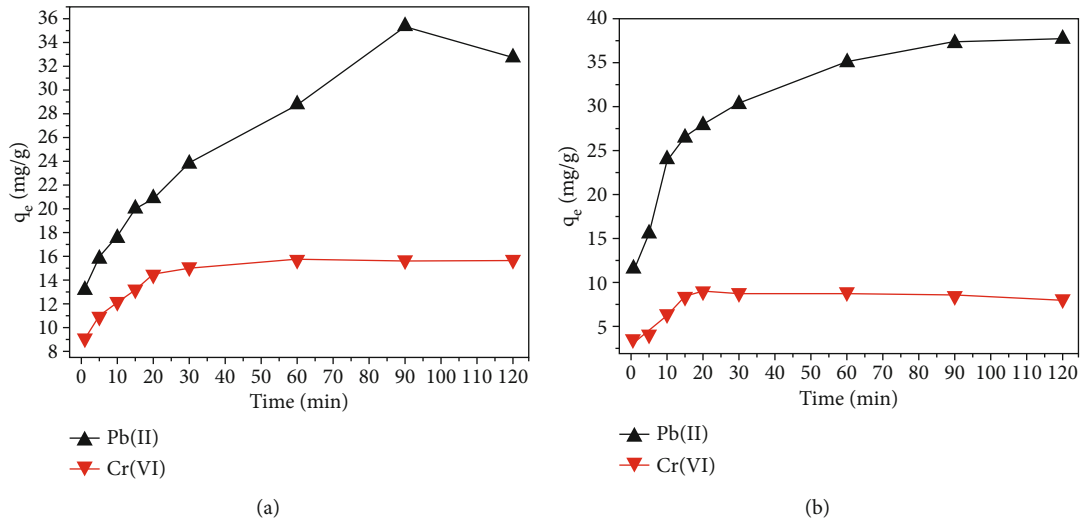

Figure 6: Time effect onto (a) PNS and (b) FNS composites of Pb(II) ions and Cr(VI) sorption. Experimental conditions: volume of solution (40 mL), concentration (100 ppm), adsorbent dosage (0.1 g), temperature of the system (298 K), agitation rate (200 rpm), and pH of solutions during Pb(II) ions and Cr(VI) sorption (5).

Table 3: Kinetic models and their parameters.

Models		FNS		PNS	
		Pb(II)	Cr(VI)	Pb(II)	Cr(VI)
PFO	q_e (mgg^{-1})	35.20	8.64	30.98	14.15
	K_1 (m^{-1})	0.10	0.17	0.07	0.96
	r^2	0.9979	0.9938	0.9947	0.9976
PSO	q_e (mgg^{-1})	33.24	18.32	23.71	20.67
	K_2 (gmg^{-1} min^{-1})	0.0377	0.1370	0.0419	0.0743
	r^2	0.9024	0.8481	0.7415	0.8969
IPD	C	15.48	4.11	13.09	9.06
	K_i (g g^{-1} min$^{0.5}$)	1.7716	0.4202	2.3475	0.6298
	r^2	0.917	0.719	0.941	0.876
EPA	%	59.00	53.92	62.98	42.48
ESA	%	41.00	46.08	37.02	57.52
Experimental (q_e) (mgg^{-1})		37.76	8.92	35.36	15.75

EPA: estimated pore sorption; ESA: estimated surface sorption.

0.935, respectively. This indicated that Pb(II) ions adsorption was best described by Freundlich than Langmuir isotherm which suggested that the surface was heterogeneous and also the ions bind physically and form multilayer [46]. However, isotherm data of Cr(VI) ions onto PNS and FNS composites showed a high (r^2) value of 0.997 and 0.995, respectively, for Langmuir which demonstrated the formation of a homogenous monolayer.

3.2.4. Time Effect and Adsorption Kinetics. The sorption rates of Cr(VI) and Pb(II) ions were studied in the time intervals of 1-120 min as shown in Figures 6(a) and 6(b). The sorption rate of Cr(VI) ions was faster than Pb(II) ions for both PNS and FNS composites as shown in Figures 5(a) and 5(b). The maximum sorption for Cr(VI) ions was reached in 20 min in both Figures 5(a) and 5(b); meanwhile, the adsorption rate of Pb(II) ions was slow and continue increasing up to 90 min of reaction. The slow adsorption stage was caused by the low concentration gradients then finally produced the equilibrium condition [71]. An increase in metal ions adsorption was observed in both adsorbents due to probability of Cr(VI) and Pb(II) ions occupying vacant sites on the adsorbents, because there were plenty of unsaturated vacant sites that resulted in quick initial adsorption [9, 72]. However, as time continues, vacant sites get exhausted and saturated therefore sorption ability of PNS and FNS composites decreased until equilibrium or decrease in sorption capacity. The maximum adsorption capacities of PNS composite for Cr(VI) and Pb(II) were found to be 15.75 and 35.36 mg/g, respectively, and FNS composites were 8.92 and 37.76 mg/g for Cr(VI) and Pb(II), respectively. These capacities were obtained under the following experimental conditions: 40 mL of solution at a temperature of 298 K using an adsorbent dosage of 0.1 g with a concentration of 100 ppm at pH.

The kinetic study of PNS and FNS composites in removing Cr(VI) and Pb(II) ions was estimated using pseudo-first order (PFO) and pseudo-second order (PSO). The adsorption capacity (q_e), rate constants (k_1 and k_2), and correlation coefficient (r^2) values are shown in Table 3. The adsorption process was estimated based on the correlation coefficient value that is closer to unity (1). The data showed that (r^2) values of PFO model for PNS and FNS composites for both Cr(VI) and Pb(II) ions were ranging from 0.993 to 0.997 which was close to 1, whilst the (r^2) for PSO ranged from 0.741 to 0.902. Therefore, the good fit for PFO data suggested that a physisorption mechanism was involved for all adsorbents fitting in PFO. The removal uptake of Cr(VI) and Pb(II) ions was also assessed using intraparticle diffusion (IPD) kinetic model by determining whether the sorption process has occurred through estimated surface adsorption (ESA) or estimated pores adsorption (EPA). The sorption of Cr(VI) and Pb(II) ions onto FNS composite occurred through pore

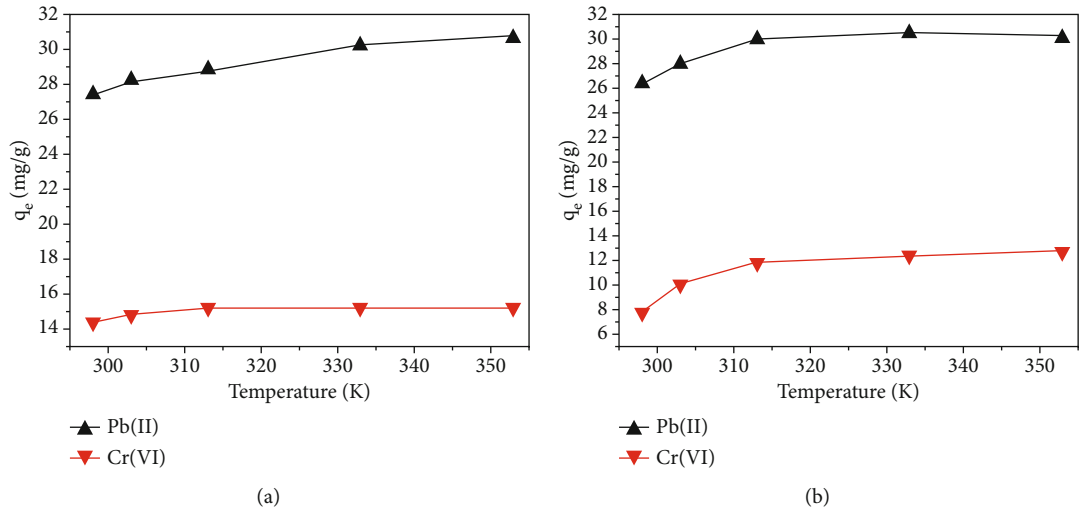

Figure 7: Temperature effect (a) PNS and (b) FNS composites of Pb(II) ions and Cr(VI) sorption. Experimental conditions: volume of solution (40 mL), time (60 min), adsorbent dosage (0.1 g), concentration (100 ppm), agitation rate (200 rpm), and pH of solutions during Pb(II) ions and Cr(VI) sorption (5).

Table 4: Thermodynamic studies and their parameters.

Parameter	FNS		PNS	
	Pb(II)	Cr(VI)	Pb(II)	Cr(VI)
ΔH° (KJ mol^{-1})	$8x10^{-4}$	$7x10^{-4}$	$1x10^{-3}$	$1x10^{-3}$
ΔS° (KJ mol^{-1} K^{-1})	$3x10^{-3}$	$1x10^{-3}$	$3x10^{-3}$	$2x10^{-3}$
ΔG° (KJ mol^{-1})				
298 K	-1.70	-4.66	-1.43	-1.19
303 K	-5.02	-4.76	-3.28	-1.26
313 K	-5.96	-4.92	-4.17	-1.36
333 K	-6.18	-5.78	-5.84	-1.67
353 K	-7.06	-5.07	-7.99	-1.44

adsorption with percentages of 59.00 and 53.92%, respectively. Similarly, the sorptions of Cr(VI) and Pb(II) ions onto PNS composite were 42.48 and 62.98%, respectively.

3.2.5. Temperature and Thermodynamic Parameters. Figures 7(a) and 7(b) show the effects of temperature on sorption on PNS and FNS composites. The graphs showed that the adsorption of Cr(VI) and Pb(II) ions is temperature dependent. The adsorption of Cr(VI) ions on both adsorbents showed an increase in sorption capacity with increased temperature between 298 and 313 K in Figures 6(a) and 6(b). At higher temperatures beyond 313 K, no further increase of adsorption was observed; instead, equilibrium was attained for both adsorbents. This suggests that the heat of adsorption of Cr(VI) ions onto FNS and PNS composite was small; hence, changing the temperature could not change the thermodynamics of the system which may imply that only slight energy was needed to break the repulsive forces hindering the Cr(VI) ions adsorption [10]. Further increase in temperature to 308 K also confirmed that the adsorption process was physical [73]. A different trend was observed for Pb(II) ions on PNS composite in Figure 6(a), whereby the adsorption capacity increased as the temperature increased from 298 to 353 K. However, the sorption of Pb(II) ions onto FNS composite in Figure 6(b) only increased as temperature increased from 298 to 313 K thereafter reached equilibrium. The uptake capacity increased with increasing the temperature on both adsorbents. This suggested that the reaction was endothermic and the increase in adsorption capacity was perhaps due to the diffusion and increase in the number of binding sites developed as a result of the breakage of internal bonds [41, 74]. The maximum adsorption capacities of PNS at room temperature were 15.21 mg/g for Cr(VI) ions and 30.66 mg/g for Pb(II) ions. On the other hand, the sorption capacities of FNS were 12.76 and 30.54 mg/g for Cr(VI) and Pb(II) ions, respectively. These results were obtained using an adsorbent dosage of 0.1 g with a solution volume of 40 mL for 60 min at pH of 5 and 100 ppm working solution.

The determination of thermodynamic parameters is very important in order to determine spontaneity and the heat change of the adsorption reactions. Thermodynamic parameters, namely enthalpy (ΔH°), entropy (ΔS°), and Gibb's free energy (ΔG°) changes of adsorption, are shown in Table 4. The negative values of (ΔG°) indicate the feasibility of the adsorption process, physical characteristics nature of the process, and the spontaneous nature of the sorption towards Cr(VI) and Pb(II) ions onto PNS and FNS composite [75, 76]. The magnitude of the Gibbs free energy for Pb(II) ions onto PNS and FNS composite becomes more negative when temperature increased from 298 to 353 K; this suggests that the adsorption process was favourable at higher temperature [77].

The positive values of (ΔS°) indicated the randomness at solid or solution interfaces during the adsorption of Cr(VI) and Pb(II) ions onto both PNS and FNS composite [78]. The positive values of (ΔH°) showed the endothermic nature of the adsorption process which may also support a slight increase in value of Pb(II) ions uptake of the adsorbents with the rise in temperature [76].

Table 5: Maximum sorption capacities of previously reported various adsorbents for Cr(VI) ions.

Adsorbent	Maximum capacity (mg/g)	Solution pH	Temperature (°C)	Reference
Iron oxide nanoparticles	45.0	1	25	Burks et al., [89]
Fe_3O_4 nanoparticles	26.5	2	25	Liang et al., [90]
Activated Iron bamboo biochar	25.7	2	25	He et al., [50]
Fe^{3+}/Fe^{2+} black cumin seeds	15.75	5	25	This study
Magnetite-pine composite	13.9	2	25	Pholosi et al., [91]
Banana waste	10.0	2	28	Sharma et al., [92]
Starch-based iron oxide	9.0	2	25	Singh et al., [93]
Activated carbon mango	7.80	2	35	Rai et al., [94]
Activated bamboo biochar	5.4	2	25	He et al., [50]
Peapod	4.3	2	28	Sharma et al., [92]
Carbon nanotubes	2.5	9	50	Mubarak et al., [95]

3.2.6. Physicochemical Studies of the Adsorbents. The effect of pH can also be explained in terms of $pH_{(PZC)}$ of PNS and FNS composites. The point of zero charge is described as the point at which the surface basic or acidic functional groups no longer contribute to the pH value of the solution. The points of zero charge $pH_{(PZC)}$ of PNS and FNS composites were 2.15 and 3.00, respectively. These results indicated that the surface of the PNS and FNS composites was acidic.

4. Comparative Studies of Cr(VI) and Pb(II) Ions

The modified *Nigella Sativa* adsorbents of PNS and FNS composite adsorption capacities for Cr(VI) and Pb(II) ions were compared with other affordable adsorbents materials reported in literature. The comparison studies as shown in Tables 1 and 5 of both adsorbents showed higher performance than some of the reported adsorbents for Cr(VI) and Pb(II) ions adsorption. Therefore, PNS and FNS composites are promising low-cost adsorbents for Cr(VI) and Pb(II) ions removal from aqueous solution.

5. Conclusion

FNS and PNS composites were prepared and used as adsorbents to investigate the influence of surface modification and be used for the adsorption of Cr(VI) and Pb(II) ions. Sucrose and iron oxide were combined with *Nigella Sativa* seeds to prepare FNS composites. The composites were prepared by precipitation and characterized with XRD and FTIR. To investigate the adsorption efficiency of the prepared iron oxide composites for the removal of Cr(VI) and Pb(II) ions, batch adsorption studies were carried out under different parameters. The maximum adsorption capacities for Cr(VI) were 15.6 and 13.0 mg/g onto PNS and FNS composites, respectively, at pH 1. On the other hand, the maximum sorptions of Pb(II) ions were 39.7 and 37.9 mg/g onto PNS and FNS composites at pH 5. Both PNS and FNS composites capacities increased with increasing initial concentration whereby Pb(II) ions adsorbed more than Cr(VI) ions. The adsorption of Cr(VI) ions was fast within 20 and 90 min for Pb(II) ions on both adsorbents. Sorption of Cr(VI) and Pb(II) ions on both adsorbents increased with increased temperature which displayed the endothermic nature of the processes [79]. Freundlich isotherm was best fitted for both adsorbents for the sorption of Pb(II) ions and Langmuir for Cr(VI) ions. The rate of adsorption showed a good fit for pseudo-first-order kinetic model which suggested that physisorption mechanism [80] of Cr(VI) and Pb(II) ions was involved for both adsorbents. The negative free energy (ΔG°) values indicated that the process feasible and spontaneous onto PNS and FNS composites [81]. The (ΔG°) values decreased as temperature increased from 298 to 353 K which showed that the adsorption process was favourable at higher temperature. The positive values of (ΔS°) indicated the randomness of water molecules from the surface of both PNS and FNS composites. The positive values of (ΔH°) showed the endothermic nature of the adsorption process [82]. These results indicated that the easily available and affordable carbon source- (sucrose-) based *Nigella Sativa* seeds can be considered as adsorbent for removing Cr(VI) and Pb(II) ions from aqueous solution. The results showed that PNS composite had a higher adsorption capacity of 39.7 mg/g for Pb(II) and 15.6 mg/g for Cr(VI) compared to FNS composite. Therefore, PNS and FNS composites can be used as low-cost materials for the removal of Pb(II) and Cr(VI) ions from aqueous solution. The *Nigella Sativa* seeds used in this study had high uptake for Pb(II) than Cr(VI) compared to the uptake of 10.07 mg/g for methylene blue reported by [14, 15]. Other adsorption studies on magnetized *Nigella Sativa* seeds for the removal of methylene blue dye had higher uptake compared to this study [16, 17].

Data Availability

The raw data was generated at the Vaal University of Technology. The data supporting the findings of this study may be made available from the corresponding author(s) on request.

Conflicts of Interest

The authors declared there are no conflicts of interest with respect to the research, publication of this article, and authorship.

Acknowledgments

We acknowledge the supports of the National Research Fund-NRF (Grand number: 112983) for funding this work and the Department of Chemistry, Vaal University of Technology, Vanderbijlpark, South Africa.

References

[1] M. Gueye, Y. Richardson, F. T. Kafack, and J. Blin, "High efficiency activated carbons from African biomass residues for the removal of chromium(VI) from wastewater," *Journal of Environmental Chemical Engineering.*, vol. 2, no. 1, pp. 273–281, 2014.

[2] S. I. Shupack, "The chemistry of chromium and some resulting analytical problems," *Environmental Health Perspectives*, vol. 92, pp. 7–11, 1991.

[3] M. H. Dehghani, D. Sanaei, I. Ali, and A. Bhatnagar, "Removal of chromium(VI) from aqueous solution using treated waste newspaper as a low-cost adsorbent: kinetic modeling and isotherm studies," *Journal of Molecular Liquids*, vol. 215, pp. 671–679, 2016.

[4] J. Li, M. Fan, M. Li, and X. Liu, "Cr(VI) removal from groundwater using double surfactant-modified nanoscale zero-valent iron (nZVI): effects of materials in different status," *Science of the Total Environmental*, vol. 717, p. 137112, 2020.

[5] P. Chand and Y. B. Pakade, "Removal of Pb from water by adsorption on apple pomace: equilibrium, kinetics, and thermodynamics studies," *Journal of Chemistry*, vol. 2013, 8 pages, 2013.

[6] F. Alguacil, L. Alcaraz, I. García-Díaz, and F. López, "Removal of Pb^{2+} in wastewater via adsorption onto an activated carbon produced from winemaking waste," *Metals*, vol. 8, no. 697, pp. 1–15, 2018.

[7] J. E. Puzas, J. Campbell, R. J. O'Keefe, and R. N. Rosier, "Lead toxicity in the skeleton and its role in osteoporosis. Nutrition and bone health," in *Nutrition and Bone Health*, M. F. Holick and B. Dawson-Hughes, Eds., pp. 363–376, Nutrition and Bone Health. Humana Press, Totowa, NJ, 2004.

[8] R. Bardestani, C. Roy, and S. Kaliaguine, "The effect of biochar mild air oxidation on the optimization of lead(II) adsorption from wastewater," *Journal of Environmental Management*, vol. 240, pp. 404–420, 2019.

[9] N. K. Abdulla, S. I. Siddiqui, N. Tara, A. A. Hashmi, and S. A. Chaudhry, "Psidium guajava leave-based magnetic nanocomposite γ-Fe_2O_3@GL: a green technology for methylene blue removal from water," *Journal of Environmental Chemical Engineering*, vol. 7, no. 6, p. 103423, 2019.

[10] P. N. Diagboya and D. Dikio, "Scavenging of aqueous toxic organic and inorganic cations using novel facile magneto-carbon black-clay composite adsorbent," *Journal Cleaner Production*, vol. 180, pp. 71–80, 2018.

[11] R. Zhang, Z. Wang, Z. Zhou et al., "Highly effective removal of pharmaceutical compounds from aqueous solution by magnetic Zr-based MOFs composites," *Journal of Industrial Engineering Chemistry Research*, vol. 58, no. 9, pp. 3876–3884, 2019.

[12] A. Dehbi, Y. Dehmani, H. Omari, A. Lammini, K. Elazhari, and A. Abdallaoui, "Hematite iron oxide nanoparticles (α-Fe_2O_3): synthesis and modelling adsorption of malachite green," *Journal of Environmental Chemical Engineering*, vol. 8, no. 1, p. 103394, 2020.

[13] T. Chen, Q. Wang, J. Lyu, P. Bai, and X. Guo, "Boron removal and reclamation by magnetic magnetite (Fe_3O_4) nanoparticle: an adsorption and isotopic separation study," *Separation and Purification Technology*, vol. 231, p. 115930, 2020.

[14] S. I. Siddiqui and S. A. Chaudhry, "Nigella sativa plant based nanocomposite-$MnFe_2O_4$/BC: an antibacterial material for water purification," *Journal of Cleaner Production*, vol. 200, pp. 996–1008, 2018.

[15] S. I. Siddiqui and S. A. Chaudhry, "Nanohybrid composite Fe_2O_3-ZrO_2/BC for inhibiting the growth of bacteria and adsorptive removal of arsenic and dyes from water," *Journal of Cleaner Production*, vol. 223, pp. 849–868, 2019.

[16] S. I. Siddiqui, F. Zohra, and S. A. Chaudhry, "Nigella Sativa seed based nanohybrid composite- Fe_2O_3-SnO_2/BC: a novel material for enhanced adsorptive removal of methylene blue from water," *Environmental Research*, vol. 178, p. 108667, 2019.

[17] S. I. Siddiqui, O. Manzoor, M. Mohsin, and S. A. Chaudhry, "Nigella Sativa seed based nanocomposite-MnO_2/BC: an antibacterial material for photocatalytic degradation, and adsorptive removal of Methylene blue from water," *Environmental Research*, vol. 171, pp. 328–340, 2019.

[18] M. Vadi and H. Najafi, "Adsorption isotherms of (+D) sucrose on multi-wall carbon nanotube," *Oriental Journal Chemistry*, vol. 27, no. 3, pp. 1281–1284, 2011.

[19] O. V. Kuznetsov, M. X. Pulikkathara, R. F. M. Lobo, and V. N. Khabasheskua, "Solubilization of carbon nanoparticles, nanotubes, nano onions, and nanodiamonds through covalent functionalization with sucrose," *Russian Chemical Bulletin, International Edition.*, vol. 59, no. 8, pp. 2005–2008, 2010.

[20] S. Mallakpour and V. Behranvand, "Chemical adsorption of D-sucrose on MWCNTs for compatibility improvement with alanine-based poly(amide-imide) matrix: morphology examination and thermal stability study," *Colloid Polym Sci*, vol. 294, no. 1, pp. 239–246, 2016.

[21] A. Y. Orbak and I. Orbak, "Effective factor analysis for chromium (VI) removal from aqueous solutions and its application to tuncbilek lignite using design of experiments," *Journal of Chemistry*, vol. 2019, 10 pages, 2019.

[22] C. Santhosh, P. Kollu, S. Doshi et al., "Adsorption, photodegradation and antibacterial study of graphene–Fe3O4 nanocomposite for multipurpose water purification application," *RSC Advances*, vol. 4, no. 54, pp. 28300–28308, 2014.

[23] A. K. Datta, A. Saha, A. Bhattacharya, A. Mandal, R. Paul, and S. Sengupta, "Black Cumin (Nigella Sativa l.)-A review," *Journal Plant Development Sciences*, vol. 4, no. 1, pp. 1–43, 2012.

[24] A. Pugazhendhi, G. M. Boovaragamoorthy, K. Ranganathan, M. Naushad, and T. Kaliannan, "New insight into effective biosorption of lead from aqueous solution using Ralstonia solanacearum: characterization and mechanism studies," *Journal of Cleaner Production*, vol. 174, pp. 1234–1239, 2018.

[25] R. Ahmad and R. S. Haseeb, "Black cumin seed (BCS): a non conventional adsorbent for the removal of Cu (II) from

aqueous solution," *Desalination Water Treatment*, vol. 56, pp. 2512–2521, 2014.

[26] S. I. Siddiqui, G. Rathi, and S. A. Chaudhry, "Acid washed black cumin seed powder preparation for adsorption of methylene blue dye from aqueous solution: thermodynamic, kinetic and isotherm studies," *Journal of Molecular Liquids*, vol. 264, pp. 275–284, 2018.

[27] M. S. Al Jassir, A. Shaker, and M. A. Khaliq, "Deposition of heavy metals on green leafy vegetables sold on roadsides of Riyadh City, Saudi Arabia," *Bulletin of Environmental Contamination and Toxicology*, vol. 75, no. 5, pp. 1020–1027, 2005.

[28] S. I. Siddiqui, S. A. Chaudhry, and S. U. Islam, "Green adsorbents from plant sources for the removal of arsenic: an emerging wastewater treatment technology," in *Plant-Based Natural Products: Derivatives and Applications*, S. U. Islam, Ed., pp. 193–215, John Wiley Sons Inc, New York, 2017.

[29] S. I. Siddiqui and S. A. Chaudhry, "Iron oxide and its modified forms as an adsorbent for arsenic removal: a comprehensive recent advancement," *Process Safety and Environmental Protection*, vol. 111, pp. 592–626, 2017.

[30] E. Esmaeili, M. Salavati-Niasari, F. Mohandes, F. Davar, and H. Seyghalkar, "Modifie single-phase hematite nanoparticles via a facile approach for large-scale synthesis," *Chemical Engineering Journal*, vol. 170, no. 1, pp. 278–285, 2011.

[31] M. S. Niasari, F. Davar, and M. Mazaheri, "Synthesis and characterization of ZnS nanoclusters via hydrothermal processing from [bis(salicylidene)zinc(II)]," *Journal Alloys and Compounds*, vol. 470, no. 1-2, pp. 502–506, 2009.

[32] D. L. Sivadas, S. Vijayan, R. Rajeev, K. N. Ninan, and K. Prabhakaran, "Nitrogen-enriched microporous carbon derived from sucrose and urea with superior CO_2 capture performance," *Carbon*, vol. 109, pp. 7–18, 2016.

[33] R. Dubey, J. Bajpai, and A. Bajpai, "Green synthesis of graphene sand composite (GSC) as novel adsorbent for efficient removal of Cr (VI) ions from aqueous solution," *Journal of Water Process Engineering*, vol. 5, pp. 83–94, 2015.

[34] J. Goscianska, M. Marciniak, and R. Pietrzak, "Ordered mesoporous carbons modified with cerium as effective adsorbents for azo dyes removal," *Separation and Purification Technology*, vol. 154, pp. 236–245, 2015.

[35] K. C. Bedin, A. C. Martins, A. L. Cazetta, O. Pezoti, and V. C. Almeida, "KOH-activated carbon prepared from sucrose spherical carbon: adsorption equilibrium, kinetic and thermodynamic studies for methylene blue removal," *Chemical Engineering Journal*, vol. 286, pp. 476–484, 2016.

[36] M. Behjati, M. Baghdadi, and A. Karbassi, "Removal of mercury from contaminated saline wasters using dithiocarbamate functionalized-magnetic nanocomposite," *Journal of Environmental Management*, vol. 213, pp. 66–78, 2018.

[37] I. Langmuir, "The adsorption of gases on plane surfaces of glass, mica and platinum," *Journal of the American Chemical Society*, vol. 40, no. 9, pp. 1361–1403, 1918.

[38] H. M. F. Freundlich, "Over the adsorption in solution," *Journal of Physical Chemistry*, vol. 57, pp. 385–471, 1906.

[39] Y. Ho and G. McKay, "Pseudo-second order model for sorption processes," *Process Biochemistry*, vol. 34, no. 5, pp. 451–465, 1999.

[40] J. W. Weber, J. C. Morris, and J. Sanit, "Kinetics of adsorption carbon from solutions," *Journal of the Sanitary Engineering Division*, vol. 89, no. 2, pp. 31–60, 1963.

[41] Z. Liu and F. S. Zhang, "Removal of lead from water using biochars prepared from hydrothermal liquefaction of biomass," *Journal of Hazardous Materials*, vol. 167, no. 1-3, pp. 933–939, 2009.

[42] R. N. Oliveira, M. C. Mancini, F. C. S. de Oliveira et al., "FTIR analysis and quantification of phenols and flavonoids of five commercially available plants extracts used in wound healing," *Revista Materia*, vol. 21, no. 3, pp. 767–779, 2016.

[43] N. D. Shooto, P. M. Thabede, and E. B. Naidoo, "Simultaneous adsorptive study of toxic metal ions in quaternary system from aqueous solution using low cost black cumin seeds (Nigella sativa) adsorbents," *South African Journal Chemical Engineering*, vol. 30, pp. 15–27, 2019.

[44] M. Husseien, A. A. Amer, A. El-Maghraby, and N. Hamedallah, "A comprehensive characterization of corn stalk and study of carbonized corn stalk in dye and gas oil sorption," *Journal Analytical and Applied Pyrolysis*, vol. 86, no. 2, pp. 360–363, 2009.

[45] T. Matos, J. Schultz, M. Khan et al., "Using magnetized (Fe_3O_4/biochar nanocomposites) and activated biochar as adsorbents to remove two neuro-active pesticides from waters," *Journal of the Brazilian Chemistry Society*, vol. 28, no. 10, pp. 1975–1987, 2017.

[46] P. M. Thabede, N. D. Shooto, T. Xaba, and E. B. Naidoo, "Sulfuric activated carbon of black cumin (Nigella sativa L.) seeds for the removal of cadmium(II) and methylene blue dye," *Asian Journal of Chemistry*, vol. 32, no. 6, pp. 1361–1369, 2020.

[47] Y. Li, S. Pan, Q. Yu, X. Ding, and R. Liu, "Adsorption mechanism and electrochemical performance of methyl blue onto magnetic $Ni_{(1-x-y)}Co_yZn_xFe_2O_4$ nanoparticles prepared via the rapid-combustion process," *Ceramics International*, vol. 46, no. 3, pp. 3614–3622, 2020.

[48] V. E. Pakade, T. D. Ntuli, and A. E. Ofomaja, "Biosorption of hexavalent chromium from aqueous solutions by Macadamia nutshell powder," *Applied Water Science*, vol. 7, no. 6, pp. 3015–3030, 2017.

[49] M. Lesaoana, R. P. V. Mlaba, F. M. Mtunzi, M. J. Klink, P. Ejidike, and V. E. Pakade, "Influence of inorganic acid modification on Cr(VI) adsorption performance and the physicochemical properties of activated carbon," *South African Journal Chemical Engineering*, vol. 28, pp. 8–18, 2019.

[50] R. He, X. Yuan, Z. Huang et al., "Activated biochar with iron-loading and its application in removing Cr (VI) from aqueous solution," *Colloids Surfaces A*, vol. 579, p. 123642, 2019.

[51] R. Acharya, B. Naik, and K. Parida, "Cr(VI) remediation from aqueous environment through modified-TiO_2-mediated photocatalytic reduction," *Beilstein Journal of Nanotechnology*, vol. 9, pp. 1448–1470, 2018.

[52] N. Unceta, F. Séby, J. Malherbe, and O. F. X. Donard, "Chromium speciation in solid matrices and regulation: a review," *Analytical and Bioanalytical Chemistry.*, vol. 397, no. 3, pp. 1097–1111, 2010.

[53] J. Zhang, S. Lin, M. Han, Q. Su, L. Xia, and Z. Hui, "Adsorption properties of magnetic magnetite nanoparticle for coexistent Cr(VI) and Cu(II) in mixed solution," *Water*, vol. 12, no. 2, p. 446, 2020.

[54] R. Acharya, S. Martha, and K. M. Parida, "Remediation of Cr(VI) using clay minerals, biomasses and industrial wastes as adsorbents," in *Advanced Materials for Waste Water Treatment*, S. Islam, Ed., pp. 129–170, John Wiley and Sons, Inc, New York, 2017.

[55] C. V. Gherasim, G. Bourceanu, R. I. Olariu, and C. Arsene, "A novel polymer inclusion membrane applied in chromium (VI) separation from aqueous solutions," *Journal of Hazardous Materials*, vol. 197, pp. 244–253, 2011.

[56] B. Dhal, H. N. Thatoi, N. N. Das, and B. D. Pandey, "Chemical and microbial remediation of hexavalent chromium from contaminated soil and mining/metallurgical solid waste: a review," *Journal of Hazardous Materials*, vol. 250, no. 251, pp. 272–291, 2013.

[57] L. C. Maremeni, S. J. Modise, F. M. Mtunzi, M. J. Klink, and V. E. Pakade, "Adsorptive removal of hexavalent chromium by diphenylcarbazide-grafted macadamia nutshell powder," *Bioinorganic Chemistry and Applications*, vol. 2018, 14 pages, 2018.

[58] M. J. Jorge, M. C. Nilson, H. R. Aracely, and F. Machuca-Martínez, "Data on the removal of metals (Cr^{3+}, Cr^{6+}, Cd^{2+}, Cu^{2+}, Ni^{2+}, Zn^{2+}) from aqueous solution by adsorption using magnetite particles from electrochemical synthesis," *Data in Brief*, vol. 24, p. 103956, 2019.

[59] C. d. G. Sampaio, L. S. Frota, H. S. Magalhães et al., "Chitosan/mangiferin particles for Cr(VI) reduction and removal," *International Journal of Biological Macromolecules*, vol. 78, pp. 273–279, 2015.

[60] L. S. McNeill, J. E. McLean, J. L. Parks, and M. A. Edwards, "Hexavalent chromium review, part 2: chemistry, occurrence, and treatment," *Journal-American Water Works Association*, vol. 104, no. 7, pp. E395–E405, 2012.

[61] A. Bhowal and S. Datta, "Studies on transport mechanism of Cr(VI) extraction from an acidic solution using liquid surfactant membranes," *The Journal of Membrane Science*, vol. 188, no. 1, pp. 1–8, 2001.

[62] L. Yang and J. Chen, "Biosorption of hexavalent chromium onto raw and chemically modified _Sargassum_ sp.," *Bioresource Technology*, vol. 99, no. 2, pp. 297–307, 2008.

[63] M. Shahid, C. Dumat, M. Aslam et al., "Assessment of lead speciation by organic ligands using speciation models," *Chemical Speciation Bioavailability*, vol. 24, no. 4, pp. 248–252, 2012.

[64] L. M. Vera, D. Bermejo, M. F. Uguña, N. Garcia, M. Flores, and E. González, "Fixed bed column modeling of lead(II) and cadmium(II) ions biosorption on sugarcane bagasse," *Environmental Engineering Research*, vol. 24, no. 1, pp. 31–37, 2019.

[65] O. A. Lukanin, B. N. Ryzhenko, and N. A. Kurovskaya, "Zn and Pb solubility and speciation in aqueous chloride fluids at T-P parameters corresponding to granitoid magma degassing and crystallization," *Geochemistry International*, vol. 51, no. 10, pp. 802–830, 2013.

[66] R. A. Easley and R. H. Byrne, "The ionic strength dependence of lead (II) carbonate complexation in perchlorate media," *Geochimica et Cosmochimica Acta*, vol. 75, no. 19, pp. 5638–5647, 2011.

[67] P. A. Nikolaychuk, "The revised potential-pH diagram for Pb-H_2O system," *Ovidius University Annals of Chemistry*, vol. 29, no. 2, pp. 55–67, 2018.

[68] X. Wang, L. Wang, Y. Wang et al., "Calcium sulfate hemihydrate whiskers obtained from flue gas desulfurization gypsum and used for the adsorption removal of lead," *Crystals*, vol. 7, no. 9, p. 270, 2017.

[69] M. Silwamba, M. Ito, N. Hiroyoshi et al., "Recovery of lead and zinc from zinc plant leach residues by concurrent dissolution-cementation using zero-valent aluminum in chloride medium," *Metals*, vol. 10, no. 531, pp. 1–15, 2020.

[70] K. Rouibah, A.-H. Meniai, M. T. Rouibah, L. Deffous, and M. B. Lehocine, "Elimination of chromium(VI) and cadmium(II) from aqueous solutions by adsorption onto olive stones," *Open Chemical Engineering Journal*, vol. 3, no. 1, pp. 41–48, 2009.

[71] A. Aichour and H. Zaghouane-Boudiaf, "Highly brilliant green removal from wastewater by mesoporous adsorbents: kinetics, thermodynamics and equilibrium isotherm studies," *Microchemical Journal*, vol. 146, pp. 1255–1262, 2019.

[72] N. D. Shooto, E. B. Naidoo, and M. Maubane, "Sorption studies of toxic cations on ginger root adsorbent," *Journal Industrial and Engineering Chemistry*, vol. 76, pp. 133–140, 2019.

[73] Y. Dong, B. Lu, S. Zang, J. Zhao, X. Wang, and Q. Cai, "Removal of methylene blue from coloured effluents by adsorption onto SBA-15," *Journal of Chemistry Technology Biotechnology*, vol. 86, no. 4, pp. 616–619, 2011.

[74] Y. Bagbi, A. Sarswat, D. Mohan, A. Pandey, and P. R. Solanki, "Lead (Pb^{2+}) adsorption by monodispersed magnetite nanoparticles: surface analysis and effects of solution chemistry," *Journal of Environmental Chemical Engineering*, vol. 4, pp. 237–4247, 2016.

[75] A. Oussalah, A. Boukerroui, A. Aichour, and B. Djellouli, "Cationic and anionic dyes removal by low-cost hybrid alginate/-natural bentonite composite beads: Adsorption and reusability studies," *International Journal of Biological Macromolecules*, vol. 124, pp. 854–862, 2019.

[76] N. H. Yarkandi, "Removal of lead (II) from waste water by adsorption," *International Journal of Current Microbiology Applied Science*, vol. 3, no. 4, pp. 207–228, 2014.

[77] M. H. Rodiguez, J. Yperman, R. Carleer et al., "Adsorption of Ni(II) on spent coffee and coffee husk based activated carbon," *Journal of Environmental Chemical Engineering*, vol. 6, no. 1, pp. 1161–1170, 2018.

[78] M. Mohapatra and S. Anand, "Studies on sorption of Cd(II) on Tata chromite mine overburden," *Journal of Hazardous Materials*, vol. 148, no. 3, pp. 553–559, 2007.

[79] L. Tan, H. Dong, X. Liu, J. He, H. Xu, and J. Xie, "Mechanism of palladium(II) biosorption by Providencia vermicola," *RSC Advances*, vol. 7, no. 12, pp. 7060–7072, 2017.

[80] A. Yildirim and H. Acay, "Biosorption studies of mushrooms for two typical dyes," *Journal of the Turkish Chemical Society*, vol. 7, no. 1, pp. 295–306, 2020.

[81] J. N. Edokpayi, S. S. Ndlovu, and J. O. Odiyo, "Characterization of pulverized Marula seed husk and its potential for the sequestration of methylene blue from aqueous solution," *BMC Chemistry*, vol. 13, no. 1, p. 10, 2019.

[82] S. Nethaji, A. Sivasamy, and A. B. Mandal, "Adsorption isotherms, kinetics and mechanism for the adsorption of cationic and anionic dyes onto carbonaceous particles prepared from juglans regia shell biomass," *International journal of Environmental Science and Technology*, vol. 10, pp. 231–242, 2012.

[83] A. A. Edathil, I. Shittu, J. H. Zain, F. Banat, and M. A. Haija, "Novel magnetic coffee waste nanocomposite as effective bioadsorbent for Pb(II) removal from aqueous solutions," *Journal of Environmental Chemical Engineering*, vol. 6, no. 2, pp. 2390–2400, 2018.

[84] D. Mohan, P. Singh, A. Sarswat, P. H. Steele, and C. U. Pittman Jr., "Lead sorptive removal using magnetic and nonmagnetic fast pyrolysis energy cane biochars," *Journal of Colloid and Interface Science*, vol. 448, pp. 238–250, 2015.

[85] B. Guo, F. Deng, Y. Zhao, X. Luo, S. Luo, and C. Au, "Magnetic ion-imprinted and -SH functionalized polymer for selective

removal of Pb(II) from aqueous samples," *Applied Surface Science*, vol. 292, pp. 438–446, 2014.

[86] S. Pap, V. Bezanovic, J. Radonic et al., "Synthesis of highly-efficient functionalized biochars from fruit industry waste biomass for the removal of chromium and lead," *Journal of Molecular Liquids*, vol. 268, pp. 315–325, 2018.

[87] M. Irani, M. Amjadi, and M. A. Mousavian, "Comparative study of lead sorption onto natural perlite, dolomite and diatomite," *Chemical Engineering Journal*, vol. 178, pp. 317–323, 2011.

[88] Z. Kariuki, J. Kiptoo, and D. Onyanch, "Biosorption studies of lead and copper using rogers mushroom biomass 'Lepiota hystrix'," *South African Journal of Chemical Engineering*, vol. 23, pp. 62–70, 2017.

[89] T. Burks, M. Avila, F. Akhtar et al., "Studies on the adsorption of chromium(VI) onto 3-Mercaptopropionic acid coated superparamagnetic iron oxide nanoparticles," *Journal of Colloid and Interface Science*, vol. 425, pp. 36–43, 2014.

[90] S. Liang, S. Shi, H. Zhang et al., "One-pot solvothermal synthesis of magnetic biochar from waste biomass: formation mechanism and efficient adsorption of Cr(VI) in an aqueous solution," *Science of the Total Environment*, vol. 695, p. 133886, 2019.

[91] A. Pholosi, E. B. Naidoo, and A. E. Ofomaja, "Intraparticle diffusion of Cr(VI) through biomass and magnetite coated biomass: a comparative kinetic and diffusion study," *South African Journal of Chemical Engineering*, vol. 32, pp. 39–55, 2020.

[92] P. K. Sharma, S. Ayuba, and C. N. Tripathi, "Isotherms describing physical adsorption of Cr(VI) from aqueous solution using various agricultural wastes as adsorbents," *Cogent Engineering*, vol. 3, no. 1, p. 1186857, 2016.

[93] P. N. Singh, D. Tiwary, and I. Sinha, "Improved removal of Cr(VI) by starch functionalized iron oxide nanoparticles," *Journal of Environmental Chemical Engineering*, vol. 2, no. 4, pp. 2252–2258, 2014.

[94] M. K. Rai, G. Shahi, V. Meena et al., "Removal of hexavalent chromium Cr (VI) using activated carbon prepared from mango kernel activated with H_3PO_4," *Resource-Efficient Technologies*, vol. 2, pp. S63–S70, 2016.

[95] N. M. Mubarak, R. K. Thines, N. R. Sajuni et al., "Adsorption of chromium (VI) on functionalized and non-functionalized carbon nanotubes," *Korean Journal of Chemical Engineering*, vol. 31, no. 9, pp. 1582–1591, 2014.